



1 **Progress in investigating long-term trends in the mesosphere,**
2 **thermosphere and ionosphere**

3
4

5 Jan Laštovička

6 Institute of Atmospheric Physics, Czech Acad. Sci., 14100 Prague, Czech Republic

7
8

9 *Correspondence:* Jan Laštovička (jla@ufa.cas.cz)

10
11

12 **Abstract**

13 This article reviews main progress in investigations of long-term trends in the mesosphere,
14 thermosphere and ionosphere over the period 2018-2022. Overall this progress may be
15 considered significant. The research was most active in the area of trends in the mesosphere
16 and lower thermosphere (MLT). Contradictions on CO₂ concentration trends in the MLT
17 region have been solved; in the mesosphere trends do not differ statistically from trends near
18 surface. The results on temperature trends in the MLT region are generally consistent with
19 older results but develop and detailed them further. Trends in temperatures might significantly
20 vary with local time and height in the whole height range of 30-110 km. Observational data
21 indicate different wind trends in the MLT region up to sign of trend in different geographic
22 regions, which is supported by model simulations. Changes in semidiurnal tide were found to
23 differ according to altitude and latitude. Water vapor concentration was found to be the main
24 driver of positive trends in brightness and occurrence frequency of noctilucent clouds (NLC),
25 whereas cooling through mesospheric shrinking is responsible for slight decrease in NLC
26 heights. The research activity in the thermosphere was substantially lower. The negative trend
27 of thermospheric density continues without any evidence of clear dependence on solar
28 activity, which results in increasing concentration of dangerous space debris. Significant
29 progress was reached in long-term trends in the E-region ionosphere, namely in foE. These
30 trends were found to depend principally on local time up to their sign; this dependence is
31 strong at European high midlatitudes but much less pronounced at European low midlatitudes.
32 In the ionospheric F2-region very long data series (starting at 1947) of foF2 revealed very
33 weak but statistically significant negative trends. First results on long-term trends were



34 reported for the topside ionosphere electron densities (near 840 km), the equatorial plasma
35 bubbles and the polar mesospheric summer echoes. The most important driver of trends in the
36 upper atmosphere is the increasing concentration of CO₂ but other drivers also play a role.
37 The most studied one was the effect of the secular change of the Earth's magnetic field. The
38 results of extensive modeling reveal the dominance of secular magnetic change in trends in
39 foF₂, hmF₂, TEC and Te in the sector of about 50°S-20°N and 60°W-20°E. However, its
40 effect is locally both positive and negative, so in the global average this effect is negligible.
41 The first global simulation with model WACCM-X of changes of temperature excited by
42 anthropogenic trace gases simultaneously from surface to the base of exosphere provides
43 results generally consistent with observational pattern of trends. Simulation of ionospheric
44 trends over the whole Holocene was reported for the first time. Various problems of long-term
45 trend calculations are also discussed. There are still various challenges in further development
46 of our understanding of long-term trends in the upper atmosphere. The key problem is the
47 long-term trends in dynamics, particularly in activity of atmospheric waves, which affect all
48 layers of the upper atmosphere. At present we only know that these trends might be regionally
49 different, even opposite.

50

51

52 **1 Introduction**

53

54 The anthropogenic emissions of polluting substances, greenhouse gases and ozone
55 depleting substances (ODS), affect also the upper atmosphere, including the mesosphere
56 (~50–90 km), the thermosphere (~90–1000 km), and the ionosphere, which is embedded in
57 the upper atmosphere (e.g., Rishbeth and Roble 1992; Laštovicka et al., 2006). The
58 thermosphere is the operating environment of many satellites, including the International
59 Space Station, and thousands of pieces of space debris, the orbital lifetime of which depends
60 on long-term changes of thermospheric density. Propagation of Global Positioning System
61 (GPS) signals and radio communications are affected by the ionosphere, thus anthropogenic
62 changes of these high-altitude regions can affect also satellite-based technologies which are
63 increasingly important to modern life. The challenge facing upper atmosphere climate
64 scientists is to detect long-term trends and understand their primary causes, so that society can
65 mitigate potential harmful changes.

66 Greenhouse gases in the troposphere are optically thick to outgoing longwave (infrared)
67 radiation, which they both absorb and reemit back to the surface to produce the heating effect.



68 In contrast, greenhouse gases, mainly CO₂ in the much lower density upper atmosphere are
69 optically thin to outgoing infrared radiation and the other property of CO₂, strong infrared
70 emission, dominates. In-situ collisional excitation results in atmospheric thermal energy
71 readily lost to space via outgoing infrared radiation, while the absorption of radiation
72 emanating from the lower atmosphere plays only a secondary role in the energy balance. The
73 net result is that the radiatively active greenhouse gases act as cooling agents, and their
74 increasing concentrations enhance the cooling effect in the upper atmosphere. This effect of
75 greenhouse gases may be called “greenhouse cooling” (Cicerone 1990).

76 The cooling results in thermal contraction of the upper atmosphere and related significant
77 decline in thermospheric density at fixed heights, which was observed in long-term satellite
78 drag data (e.g., Emmert et al. 2008). Downward displacement of ionospheric layers should
79 accompany this contraction. The cooling also affects chemical reaction rates and, thus, the
80 chemistry of minor constituents, resulting in further changes to the ionosphere.

81 Investigations of long-term changes in the upper atmosphere and ionosphere began with
82 the pioneering study of Roble and Dickinson (1989). They suggested that global cooling will
83 occur in the upper atmosphere due to the long-term increase of greenhouse gas
84 concentrations, particularly carbon dioxide (CO₂). Modeling studies by Rishbeth (1990) and
85 Rishbeth and Roble (1992) broadened these results to the thermosphere-ionosphere system.
86 First observational studies of long-term trends in the ionosphere were those by Aikin et al.
87 (1991) and by Laštovička and Pancheva (1991).

88 With the increasing amount of observational and model results and findings, a global
89 pattern of trend behavior began to emerge, and, in 2006, the first global scenario of trends in
90 the upper atmosphere and ionosphere was constructed (Laštovička et al., 2006a, 2008a). Since
91 2006 other parameters were added to this scenario, some discrepancies were removed and/or
92 explained, and in recent years it became increasingly clear that non-CO₂ drivers also play an
93 important role in long-term trends in the upper atmosphere and ionosphere together with the
94 dominant increasing atmospheric concentration of greenhouse gases, mainly of CO₂.

95 Various papers summarizing and discussing long-term trends and various aspects of their
96 investigations have been published in recent years. Laštovička (2017) summarized progress in
97 investigating long-term trends in the mesosphere, thermosphere and ionosphere in the period
98 2013-2016. Laštovička and Jelínek (2019) summarized and discussed problems associated
99 with calculating long-term trends in the upper atmosphere (see section 2).

100 Danilov and Konstantinova (2020a) reviewed long-term variations in the middle and upper
101 atmosphere and in ionosphere. The middle atmosphere cooling trend has reliably been



102 established from observations by different methods. On the other hand, there are noticeable
103 discrepancies in estimates of negative trends in the critical frequency foF2, which corresponds
104 to the maximum ionospheric electron density, and in its height hmF2. Processes in the
105 mesosphere and thermosphere have been more rapid than predicted by models.

106 Elias et al. (2022) reviewed long-term trends in the equatorial ionosphere due to the
107 secular variation of the Earth's magnetic field. This effect occurs in the F2 layer of the
108 ionosphere; in lower levels it is negligible. Low and equatorial latitudes are more sensitive to
109 the secular change of the Earth's magnetic field than middle latitudes.

110 Laštovička (2022) reviewed trends in foF2 from the point of view of space climate. These
111 trends are relatively weak. Different methods of trend determination and of reduction of effect
112 of solar cycle result in differences in trends in foF2.

113 Danilov and Berbenova (2021) reviewed applied aspects of long-term trends in the upper
114 atmosphere. Increasing H₂O concentration in the middle atmosphere can affect the state of
115 ozone layer and also polar mesospheric summer echoes (PMSE) with some military
116 consequences. Modifications of systems of winds and intensification of upward penetration of
117 gravity waves into the ionosphere could result in intensification of "meteorological control"
118 of ionosphere. Thermospheric cooling and related decrease of thermospheric density at
119 satellite altitudes prolong orbital lifetime of space debris and thus increase the probability of
120 dangerous collisions of space vehicles with space debris. Trends of the total electron content
121 (in unit column, TEC) and ionospheric slab thickness are related to corrections of positioning
122 systems. Trends in foF2 affect propagation of short radio waves.

123 Here I report progress in the long-term trend investigations in the mesosphere,
124 thermosphere and ionosphere over the period 2018-2022. Section 2 deals with problems in
125 calculating long-term trends. Section 3 treats trends in the mesosphere and lower
126 thermosphere. Section 4 describes progress in studying thermospheric trends. Section 5 deals
127 with long-term trends in the ionosphere. Section 6 treats progress in global or very-long-term
128 modeling. Section 7 deals with roles of non-CO₂ drivers of trends. Section 8 contains
129 conclusions.

130

131

132 **2 Problems in Calculating Long-Term Trends**

133

134 Laštovička and Jelínek (2019) summarized and discussed problems associated with
135 calculating long-term trends in the upper atmosphere. Calculations of long-term trends in the



136 upper atmosphere suffer with various problems, which may be divided into three groups: (1)
137 natural variability, (2) data problems, and (3) methodology. These problems have often been
138 underestimated in trend calculations in the past, which lead to controversial trend results. In
139 the upper atmosphere there is a strong influence of the 11-year solar cycle, which has to be
140 removed as much as possible. Different solar activity proxies used may result in clearly
141 different trends, particularly for foF2 (e.g., Laštovička, 2021b), as it is illustrated by Fig. 1.
142 There are also other trend drivers (see section 7), which modify the CO₂-driven trend. A
143 serious problem of trend investigations is homogeneity of long-term data series, which should
144 be carefully checked before beginning trend calculations. The simplest method of trend
145 calculation is the linear regression method, which is however often oversimplification. Then
146 the multiple linear regression or piecewise linear regression can be applied, or more
147 sophisticated methods like artificial neural networks, machine learning, or the ensemble
148 empirical mode decomposition. Assumption of methods and their sensitivity to error
149 propagation (effects of errors in data) should be considered. The selection of suitable method
150 should be data driven. It should also be noted that trends calculated in terms of fixed heights
151 versus fixed pressure levels might be different, sometimes even substantially.

152

153 **Figure 1.**

154

155 The problem of the most suitable solar activity proxy for ionospheric investigations was
156 treated by Laštovička (2019, 2021a, 2021b). They used yearly average and monthly median
157 foF2 data of three midlatitude European stations, Juliusruh, Pruhonice and Rome and six solar
158 activity proxies, F10.7, F30, Mg II, He II, sunspot numbers and the solar H Lyman- α flux,
159 analyzed over two periods, 1976-1995 and 1996-2014. This analysis suggests F30 and Mg II
160 as the most suitable solar activity proxies, not the traditionally used proxies F10.7 and sunspot
161 numbers. Preliminary results for yearly foE (critical frequency of ionospheric E-region,
162 corresponding to its electron density maximum), based on data of stations Juliusruh and
163 Slough/Chilton, favor rather F10.7. Danilov (2021) reported that the relationship between
164 F10.7 and three other solar activity proxies, sunspot number, Mg II and Lyman- α flux, is
165 close in solar cycles 22 and 23 but differs in cycle 24, for which he suggested correction of
166 F10.7 for foF2 long-term investigations.

167 Danilov and Konstantinova (2020b) estimated foF2 trends of stations Juliusruh and
168 Boulder until 2018 and found peculiar foF2 trend changes in solar cycle 24. To get reasonable
169 foF2 trend compared to previous period, F10.7 has to be corrected with sunspot number and



170 the solar Lyman alpha flux values. Danilov and Konstantinova (2020c) found the same
171 problem and the same solution for hmF2.

172 Huang et al. (2020) claim that due to the seasonal dependence of the relationship between
173 NmF2 and solar EUV (extreme ultraviolet) irradiance the application of yearly values
174 (average from monthly average values) to trend calculations may result both in positive or
175 negative biases. For Juliusruh, 1970-2014, they obtained trends $0.0089 \pm 0.0044 \times 10^{11} \text{ el m}^{-3}$
176 year^{-1} for yearly average values, $0.0100 \pm 0.0033 \times 10^{11}$ for monthly average values, and
177 $0.0091 \pm 0.0033 \times 10^{11}$ for bias-corrected yearly values. However, all differences between the
178 above trends are within error bars, i.e. they are not statistically significant.

179 Main progress was reached in shedding light on problems related to natural variability,
180 mainly on the critical problem of removing/suppression of effect of solar cycle using various
181 solar activity proxies, and also in specifying problems of solar cycle 24. As concerns data
182 problems, i.e. mainly homogeneity of long data series, there are various techniques how to
183 detect discontinuities and other possible problems, which are used among others in
184 climatology and meteorology, so no special techniques are needed to be developed for the
185 upper atmosphere. As concerns methodology, we may use methods developed for
186 climatological and meteorological investigations and other available techniques but as data
187 show, often it is sufficient to use simple or multi-parameter regression, because the long-trend
188 signals and signal-to-noise ratio are often substantially stronger than in the troposphere. On
189 the other hand, the amount of data available in the upper atmosphere is much smaller and data
190 series shorter than those in the troposphere.

191

192

193 **3 Mesosphere and Lower Thermosphere**

194

195 Long-term trends in various parameters have been investigated in the mesosphere and
196 lower thermosphere (altitudes about 50-120 km, MLT region). The mostly studied parameter
197 has been temperature but both zonal and meridional winds, minor constituents, noctilucent
198 clouds, water vapor concentration and some other parameters have been studied as well. We
199 begin review with observational results on trends in temperature. Many of such studies were
200 based on SABER (Sounding of the Atmosphere using Broadband Emission Radiometry)
201 observations onboard satellite TIMED (Thermosphere Ionosphere Mesosphere Energetics and
202 Dynamics).



203 The 17 years (2000-2016) long midnight spectral OH* airglow measurements at
204 Zvenigorod (56°N, 37°E) revealed a weak negative trend of mesopause region temperature of
205 -0.7 ± 0.3 K/decade (Perminov et al., 2018).

206 Continuous Na lidar measurements of nocturnal mesopause region characteristics at Fort
207 Collins (41°N, 105°W) and Logan (42°N, 112°W) over 1990-2018 revealed a cooling trend
208 larger than -2 K/decade and a decrease of the wintertime upper mesopause height (above 97
209 km) by -450 m/decade and of the lower non-winter mesopause (height below 92 km) by -130
210 m/decade. The WACCM-X (Whole Atmosphere Community Climate Model eXtended)
211 model provides similar changes of the mesopause heights caused mainly by cooling and
212 contraction of the stratosphere and lower mesosphere (Yuan et al., 2019).

213 She et al. (2019) reported results of nighttime temperature measurements by a midlatitude
214 Na lidar over 1990-2017. The height profile of the 28-year long temperature data trend begins
215 with a weak positive warming at 85 km, continues with cooling at 87(88) km with maximal
216 cooling at 92(93) km, and it turns to a warming trend at 102(100) km. Wintertime trend is
217 much cooler than summertime trend. The lidar temperature trends generally agree with
218 SABER temperatures and within error bars also with model LIMA (Leibniz-Institute Middle
219 Atmosphere Model). They also show that data sets longer than two solar cycles are necessary
220 to obtain reliable long-term trend.

221 Li et al. (2021) merged middle atmosphere temperature observations from HALOE
222 (Halogen Occultation Experiment, 1991-2005) and SABER (2002-2019) in 45°S-45°N. They
223 found stronger mesospheric cooling at the Southern Hemisphere (SH) than at the Northern
224 Hemisphere (NH), which peaks at 60-70 km with trend of -1.2 K/decade. The temperature
225 trend derived from SABER data only is by a factor of 1.5 weaker than that based on merged
226 data, which is consistent with some upper stratosphere ozone recovery after the mid-1990s.

227 Venkat Ratnam et al. (2019) carefully merged data on the middle atmosphere over India
228 obtained by various measuring techniques (rockets, High-Resolution Doppler Imager (HRDI)/
229 Upper Atmosphere Research Satellite (UARS), (HALOE)/UARS, SABER/TIMED and
230 Mesosphere-Stratosphere-Troposphere (MST) radars) over more than 25 years. The
231 observational analysis was accompanied by WACCM-X model simulations. They found
232 significant cooling trend -1.7 ± 0.5 K/decade between 30 and 80 km heights. All observed
233 changes are well captured by the WACCM-X simulations if changes in greenhouse gas
234 concentrations are included.

235 24 years of measurements of OH nightglow rotational temperature at Davis, Antarctica
236 (68°S, 78°E) revealed a cooling trend of -1.2 ± 0.51 K/decade (French et al., 2020). The



237 comparison for the last 14 years of trend with trend derived from Aura/MLS (Microwave
238 Limb Sounder) at a level of 0.00464 hPa gives very good agreement.

239 Dalin et al. (2020) reported update of long-term trends of mesopause temperature in
240 Moscow region. They observed statistically significant cooling of the summer mesopause
241 region by -2.4 ± 2.3 K/decade and an insignificant and small cooling in winter for the period
242 2000-2018.

243 Huang and Mayr (2021) analyzed zonal mean SABER temperatures over 2002-2014. They
244 found that trends might significantly vary with local time and height in the whole height range
245 of 30-110 km. Figure 2 shows that even for zonal mean temperatures the trends at 00:00,
246 06:00, 12:00 and 18:00 LT (local time) differ evidently, particularly for 12:00 and 18:00 LT
247 and above about 75 km. However, it is possible that with a longer data series available the
248 differences would be smaller.

249

250 **Figure 2**

251

252 Bailey et al. (2021) created temporal series of mesospheric temperatures and pressure
253 altitudes by combining observations from HALOE, SABER and SOFIE (Solar Occultation for
254 Ice Experiment) for June at NH and December at SH for latitudes 64° - 70° . They found a
255 robust result that the mesosphere generally cools on most heights by 1-2 K/decades in
256 response to the increasing greenhouse gas concentrations, the cooling peaking near 0.03 hPa
257 at NH and 0.05 hPa at SH. This cooling results in atmospheric shrinking by 100-200
258 m/decade. Shrinking results in reduced cooling and eventually heating near 0.005 hPa due to
259 hydrostatic contraction.

260 Zhao et al. (2020) examined global distribution and changes of monthly average
261 mesopause temperatures based on SABER measurements at latitudes 83° S- 83° N over 2002-
262 2019. They observed cooling at all latitudes ranging from ~ 0 to -0.14 K/year with mean value
263 -0.075 ± 0.043 K/year with stronger cooling on SH than on NH. At high latitudes, the cooling
264 is significant in non-summer season; there is no significant trend in summer. They observed
265 the weakest trends in 40° - 60° N and the strongest trends in 60° - 80° S.

266 Das (2021) examined SABER temperature data for long-term trends over 2003-2019 using
267 the empirical mode decomposition method. He confirmed global cooling of the middle
268 atmosphere and found long-term trends of -0.5 K/decade in the lower mesosphere and -1.0
269 K/decade in the upper mesosphere. The SH mesopause and NH stratopause exhibit stronger



270 cooling than the opposite hemisphere. The SH mesopause shows stronger cooling over Indian
271 Ocean.

272 Zhao et al. (2021) presented another analysis of SABER temperature measurements for
273 20002-2020 at heights of 20-110 km (middle atmosphere). The near-global mean temperature
274 exhibits consistent cooling trends throughout the middle atmosphere ranging from -0.28 up to
275 -0.97 K/decade.

276 Bizuneh et al. (2022) analyzed long-term mesospheric (60-100 km) variability of
277 temperature and ozone mixing ratio as measured by SABER over 2005-2020 at latitudes 5°-
278 15°N. They found negative trends in temperature and ozone in the lower mesosphere of -0.85
279 K/decade and -0.12 ppmv/decade, respectively, and positive trends in 85-100 km of 1.25
280 K/decade and 0.27 ppmv/decade, respectively. Both temperature and ozone are affected by
281 F10.7, El Niño–Southern Oscillation (ENSO, Niño 3.4 index) and the Quasi-Biennial
282 Oscillation (QBO, QBO₃₀ index).

283 Mlynczak et al. (2022) used SABER/TIMED observations over 2002-2021 to study the
284 behavior of the MLT region. They found significant cooling and contraction from 2002 to
285 2019 (solar cycle minimum) due to weaker solar cycle and increasing CO₂. The MLT
286 thickness between 1 and 10⁻⁴ hPa contracted by 1333 m, out of which 342 m can be attributed
287 to increasing CO₂. The MLT region sensitivity to CO₂ doubling was estimated -7.5 K
288 according to the observed temperature trends and CO₂ growth rate.

289 Rayleigh radar observations at Observatoire de Haute Provence, which cover four decades,
290 did not reveal any long-term change of mesospheric temperature inversion layers potentially
291 related to climate change (Ardalan et al., 2022). Only an interannual variability with quasi
292 decadal oscillations was observed.

293 The above observational analyses have been accompanied and supported by model
294 simulation analyses of long-term trends in the MLT region temperatures.

295 Qian et al. (2019) simulated trends in mesospheric temperature and winds with model
296 WACCM-X and compared them with winds observed at Collm over 1980-2014. They found a
297 global temperature trend in the mesosphere to be negative in line with observations, and
298 reaching maximum of about -1 K/decade in the middle and lower thermosphere. The
299 temperature trend becomes near none or even slightly positive in the summer upper
300 mesosphere, likely due to dynamic effects.

301 Kuilman et al. (2020) simulated the impact of CO₂ doubling on the middle atmosphere with
302 model WACCM; they found the direct mesospheric cooling to reach up to 15 K.



303 Ramesh et al. (2020b) simulated long-term (1850-2014) variability of temperature and
304 zonal wind with model WACCM-6. They confirmed CO₂ and ozone depleting substances
305 (ODS) to be the main drivers of the observed cooling of the middle atmosphere. The
306 simulated cooling was stronger in the lower mesosphere than at higher mesospheric levels.

307 Another important parameter is wind. Trends in winds, particularly in zonal wind, were
308 studied both with observations and model simulations.

309 Venkat Ratnam et al. (2019) carefully merged data on the middle atmosphere over India
310 obtained by various measuring techniques (rockets, HRDI/UARS, HALOE/UARS,
311 SABER/TIMED and MT radars) over more than 25 years. The eastward zonal wind trend was
312 large, about -5 ms⁻¹/decade, but statistically significant only in 70-80 km, which resulted in
313 change from a strong eastward in the 1970s to a weak westward in recent decade; no
314 significant trend was found in meridional wind. All observed changes are well captured by the
315 WACCM-X simulations if changes in greenhouse gas concentrations are included.

316 Meteor radar winds measured at Andenes (69.3°N, 16°E), Juliusruh (54.6°N, 13.4°E) and
317 Tavistock (43.3°N, 80.8°W) over 2002-2018 revealed annual wind tendency toward south and
318 west (up to 3 ms⁻¹/decade) for Andenes but slight opposite to negligible tendencies at
319 midlatitudes (Wilhelm et al., 2019).

320 Vincent et al. (2019) derived vertical wind velocities from the divergence of mean
321 meridional wind measured by MF (medium frequency) radar above Davis, Antarctica (69°S,
322 78°E) over 1994-2018 in the three weeks just after summer solstice. The estimated vertical
323 velocity peak values varied between 2 and 6 cm/s with significant interannual variability.
324 These peak values did not exhibit a significant long-term change but the height of wind
325 maximum displayed a statistically significant long-term decrease of about -0.6 km/decade.

326 Qian et al. (2019) simulated with model WACCM-X trends in mesospheric temperature
327 and winds and compared them with winds observed at Collm over 1980-2014. They found as
328 Figure 3 shows that trends in winds near altitude of 90 km reveal a dynamical pattern with
329 regionally both positive and negative values within about ±5 ms⁻¹/decade, which indicates
330 predominant control by dynamics. Figure 3 illustrates how complex are trends in winds and
331 how difficult is to investigate them.

332

333 **Figure 3.**

334

335 Kogure et al. (2022) focused on mechanisms of the thermospheric zonal mean wind
336 response to doubling the CO₂ concentration based on model GAIA (Ground-to-topside model



337 of Atmosphere and Ionosphere for Aeronomy) simulations. The pattern is very complex; three
338 main forces, ion drag, molecular viscosity and meridional pressure gradient, strongly
339 attenuate each other.

340 Very important parameter for processes in the upper atmosphere – ionosphere system and
341 for vertical coupling with lower lying layers is atmospheric waves, namely gravity and
342 planetary waves and tides. Unfortunately there was little activity in investigating trends in
343 wave activity.

344 Meteor radar winds measured at Andenes (69.3°N, 16°E), Juliusruh (54.6°N, 13.4°E) and
345 Tavistock (43.3°N, 80.8°W) over 2002-2018 revealed no significant trend in diurnal tides and
346 changes of semidiurnal tide, which differ according to altitude and latitude (Wilhelm et al.,
347 2019).

348 The WACCM6 model simulated trends of the diurnal migrating tide amplitude in the MLT
349 region (0.0001-0.01 hPa) for the period 1850-2014. Trends were found to be positive, mainly
350 due to the increasing concentration of CO₂ with some contribution of trend of ENSO (Ramesh
351 et al., 2020a).

352 Ramesh and Smith (2021) used WACCM6 simulations over 1850-2014 and found the
353 increasing non-migrating diurnal tide in the MLT region (0.0001-0.01 hPa) in temperature,
354 zonal and meridional winds, particularly at low and equatorial latitudes, predominantly due to
355 the increasing concentration of CO₂.

356 New results were obtained in studies of long-term trends in the MLT region composition,
357 namely in CO₂ and water vapor, and related trends in noctilucent (= polar mesospheric)
358 clouds.

359 Rezac et al. (2018) analyzed long-term trends of CO₂ based on direct SABER
360 measurements. They found that below 90 km the CO₂ trends statistically do not differ from
361 the surface/tropospheric CO₂ trends in agreement with model simulations, whereas above 90
362 km up to 110 km (top height of measurements) the CO₂ trends are slightly higher but less than
363 provided by previous analyses. This important study closed several years of discussions of
364 satellite-based trend of CO₂, which was originally reported to be higher than near surface.

365 Yu et al. (2022) studied water vapor evolution in the tropical middle atmosphere with
366 merged dataset of satellite observations over 1993-2020 and model SD-WACCM (WACCM6
367 with specified dynamics) simulations over 1980-2020. They found a relatively weak trend 0.1
368 ppmv/decade in observations and no trend in simulations. Simulations revealed periods of
369 increasing as well as decreasing mesospheric water vapor due to non-linear changes of
370 methane emissions and sometimes irregular changes in the tropical tropopause temperature.



371 Nedoluha et al. (2022) examined measurements of mesospheric water vapor by the Water
372 Vapor Millimeter-wave Spectrometers (WVMS) at three stations in California, Hawaii and
373 New Zealand from 1992 to 2021 and compared them with measurements onboard satellites by
374 HALOE, SABER and Aura/MLS. Differences between ground-based and satellite trends vary
375 within ~ 3 %/decade. This uncertainty is comparable with trends of mesospheric water vapor
376 since the early 1990s. The increase of CH_4 concentration over the last 30 years should
377 increase H_2O mixing ratio by $\sim 4\%$, which corresponds to trend 1.3 %/year. Such a trend is
378 within trends and their uncertainties derived from measurements of WVMS instruments.

379 Yue et al. (2019) report an increase of water vapor concentration in the mesosphere over
380 2002-2018 by 0.1-0.2 ppmv/decade according to SABER measurements and 0.2-0.3
381 ppmv/decade according to Aura/MLS measurements. The trend is somewhat stronger in the
382 lower and upper mesosphere. WACCM simulations provide the same trend of water vapor as
383 observations in the lower mesosphere. The origin of water vapor trend is partially dissociation
384 of methane (mainly above 65 km), and partially transport of water vapor from below.

385 On the other hand, measurements of the mesospheric water vapor concentration by the
386 radiometer MIAWARA (Middle Atmospheric WATER vapor RADIometer) in Zimmerwald
387 (46.88°N , 7.46°E) in Switzerland over 2007-2018 displayed significant decrease of water
388 vapor concentration with a rate of -0.60 ± 0.02 ppmv/decade at heights of 61-72 km (Lainer et
389 al., 2019). Authors were not able to give an explanation for the origin of the detected water
390 vapor decline.

391 A 138-years long model simulation of impact of increasing concentration of CO_2 and
392 methane near 83 km altitude revealed a substantial increase of the noctilucent cloud (NLC)
393 brightness due to $\sim 40\%$ increase of water vapor induced by increasing methane concentration
394 (Lübken et al., 2018). This increase is qualitatively consistent with polar mesospheric cloud
395 observations by satellites.

396 Lübken et al. (2021) analyzed long-term trends in mesospheric ice layers derived from
397 simulations with models LIMA and MIMAS (Mesospheric Ice Microphysics And tranSPort
398 model) over the period of 1871-2008 for middle (58°N), high (69°N) and Arctic (78°N)
399 latitudes. Increases of ice particle radii and NLC brightness with time are mainly caused by an
400 enhancement of water vapor. The negative trend of NLC heights is primarily caused by CO_2 -
401 induced cooling at lower heights.

402 Dalin et al. (2020) reported update of long-term trends in noctilucent clouds in Moscow
403 region. Trends in noctilucent clouds over 1968-2018 were small and insignificant in
404 agreement with other observations from comparable latitudes.



405 Long-term trends have been studied also in other parameters of the mesosphere and lower
406 thermosphere, in airglow, polar mesospheric summer echoes, or summer length in the MLT
407 region.

408 Huang (2018) used the 55-year long series of results of simulations by two models focused
409 on examining the effect of increasing CO₂ concentration on airglow intensity, volume
410 emission ratio (VER) and VER peak height. He found weak and opposite linear trends of
411 airglow intensities of OH(8,3), O(0,1) and O(¹S) spectral lines and of VER with increasing
412 CO₂, whereas the VER peak height strongly and out-of-phase correlated with geomagnetic
413 activity.

414 Observations of mesopause airglow emissions of O₂(A 0-1) and OH (6-2) at Zvenigorod
415 over 2000-2019 provided a trend of average yearly emissions of -3.3 ± 0.3 and -2.6 ± 0.02
416 %/year, respectively (Perminov et al., 2021), which is surprisingly strong trend.

417 Dalin et al. (2020) reported update of long-term trends in airglow emission intensity in
418 Moscow region. They found statistically significant negative trends in the intensities of O₂
419 A(0-1) and OH (6-2) airglows both in summer and winter for the period 2000-2018.

420 Based on radar observations at Andoya (69.5°N, 16.7°E) over 1994-2020, Latteck et al.
421 (2021) obtained after eliminating effects of solar and geomagnetic activity a polar
422 mesospheric summer echo trend of 3.2%/decade, which might be related to the observed
423 negative trend of mesospheric temperatures in polar latitudes.

424 Mesospheric wind measurements by specular meteor radars and partial reflection radars
425 over northern Germany (~54°N) and northern Norway (~69°N) over 2004-2020 using two
426 definitions of summer length provided a positive trend of summer length for one definition
427 and no trend for the other definition; 31 year midlatitude partial reflection radar data indicate
428 break point and non-uniform trend of summer length (Jaen et al., 2022).

429 Simulations with NASA (National Atmospheric and Space Administration) model E2.2-
430 AP reveal impact of CO₂ on the quasi-biennial oscillation (QBO). The increasing
431 concentration of CO₂ results in reduction of the QBO period (Dalla Santa et al., 2021). QBO
432 is a stratospheric phenomenon but with impact on the mesosphere.

433 The mesosphere and lower thermosphere was the most actively studied region of the upper
434 atmosphere and ionosphere system from the point of view of long-term trends. The most
435 studied parameter was temperature both due to its importance (the primary direct effect of
436 increasing concentration of CO₂ is cooling) and availability of both ground-based and
437 satellite-based data as well as of model simulations. The general pattern is cooling,
438 particularly in the mesosphere, but various observations are only mostly but not fully



439 consistent, partially maybe due to insufficient length of data series used; She et al. (2019)
440 claim that data sets longer than two solar cycles are necessary to obtain reliable long-term
441 trend. Huang and Mayr (2021) found that trends might significantly vary with local time and
442 height in the whole height range of 30-110 km but they studied data series only 13 years long.
443 Also model simulations provide general cooling, even though the WACCM simulations by
444 Qian et al. (2019) indicate that the temperature trend becomes near none or even slightly
445 positive in the summer upper mesosphere, likely due to dynamic effects. The results on
446 temperature trends are generally consistent with older results. It should be mentioned that
447 temperature trends are affected also by the stratospheric ozone behavior, which was highly
448 non-linear due to change after the mid-1990s from relatively rapid decline to much weaker
449 decline, stagnation or recovery (depending on region and altitude). Summing up we may say
450 that long-term trends in the MLT temperature are now better known and understood than
451 before 2018; our knowledge broadened and it is more detailed.

452 Other important group in the MLT region is dynamical parameters, winds and
453 atmospheric waves. Here the trend pattern is much more complex. Observational data indicate
454 different wind trends up to sign of trend in different geographic regions (e.g., Wilhelm et al.,
455 2019). Simulations (Qian et al., 2019) show that trends in winds reveal a dynamical pattern
456 with both positive and negative values. The limited activity in the area of atmospheric waves
457 was concentrated on tides. Meteor radar wind data from high/middle latitudes revealed no
458 significant trend in diurnal tides and changes of semidiurnal tide, which differ according to
459 altitude and latitude (Wilhelm et al., 2019). On the other hand simulations with WACCM6
460 provide positive trends for both migrating and non-migrating diurnal tides. Trends in
461 dynamical parameters are not well understood, which is the key problem of trend studies in
462 the upper atmosphere. They seem to be substantially regionally dependent.

463 Another group of parameters are CO₂, water vapor and noctilucent clouds. Rezac et al.
464 (2018) finally solved contradictions about evaluations of satellite measurements of
465 concentration of CO₂, which is the result of principal importance. It was found that the CO₂
466 concentration trends in the mesosphere (below 90 km) do not differ statistically from trends at
467 surface, even though they appear to be slightly larger above 90 km. Water vapor trends in the
468 mesosphere are generally positive, only in the equatorial region there is almost no trend. The
469 only exception is radiometer measurements in Switzerland with significant negative trend at
470 heights 61-72 km with unknown explanation. The origin of water vapor trend is partially
471 dissociation of methane (mainly above 65 km), and partly transport of water vapor from
472 below. As for noctilucent clouds, recent results confirm positive trends, which weaken with



473 decreasing latitude. This trend is mainly due to the increase of water vapor concentration.
474 Their height is slightly decreasing primarily due to mesospheric shrinking due to CO₂-induced
475 cooling at lower heights.

476 Long-term trends were studied also in other parameters. Airglow intensities in different
477 spectral lines have different and even opposite trends, even though negative trends dominate.
478 Polar mesospheric summer echo trend was found to be positive, which might be related to the
479 observed negative trend of mesospheric temperatures in polar latitudes. Midlatitude partial
480 reflection radar data indicate break point and non-uniform trend of mesospheric summer
481 length.

482

483

484 **4 Thermosphere**

485

486 The research activity in the field of thermospheric long-term trends has been moderate.
487 Out of five below cited papers three dealt with long-term trends in thermospheric density. The
488 negative trend of thermospheric density continues without any evidence of clear dependence
489 on solar activity. The decrease in thermospheric density will result in increasing concentration
490 of dangerous space debris on LEO (Low Earth Orbit) satellite orbits. GAIA model complex
491 simulations of trends in many thermospheric parameters predict among others a downward
492 shift and acceleration of meridional circulation and substantial reduction of semidiurnal tides;
493 both have not yet been studied observationally. Perrone and Mikhailov (2019) inferred
494 negative trends of the atomic oxygen column content in June but their method might be
495 questioned.

496 Weng et al. (2020) applied the machine-learning method to satellite drag data to search for
497 long-term trends in thermospheric density. Their trend estimates range from -1.5 to -2.0
498 %/decade between 250 and 575 km without any clear dependence on solar activity. They use
499 S10.7 instead of F10.7 to represent solar activity. Their model better captures thermospheric
500 density in the deep solar minimum 2008-2009 than previous empirical models.

501 Mlynczak et al. (2022) used SABER/TIMED observations over 2002-2021 to study the
502 behavior of MLT region. They found significant cooling and contraction from 2002 to 2019
503 (solar cycle minimum) due to weaker solar cycle and increasing CO₂. This cooling and
504 contraction of the MLT region contributes to decreasing thermospheric densities at LEO
505 satellite orbits, where it results in increasing concentration of dangerous space debris.



506 WACCM-X simulation of impact of increasing CO₂ concentration on thermospheric
507 density under low solar activity conditions reveals a 30% decrease of atmospheric density at
508 400 km with respect to year 2000 level if the Paris agreement surface warming limit 1.5°C is
509 reached. This thermospheric density decrease will result in satellite and space debris orbital
510 lifetime longer by 30% with consequent higher probability of dangerous satellite collisions
511 with space debris (Brown et al., 2021).

512 Liu et al. (2020) use GAIA model simulations to study the response of the thermosphere to
513 CO₂ doubling. They found that the thermosphere will cool by 10 K, more near solstices than
514 near equinoxes, more at summer pole than at winter pole. The meridional circulation shifts
515 downward and strongly accelerates by 5-15 m/s. Semidiurnal tides are reduced by 40-60% in
516 the whole thermosphere.

517 Perrone and Mikhailov (2019) inferred the atomic oxygen column content $n[O]_{col}$ in June
518 from June monthly medians of foF1 (critical frequency of F1 layer corresponding to its
519 maximum electron density) and foF2 of NH stations Rome, Juliusruh, Sodankylä and Boulder
520 for six solar cycles. 93% of total variance of $n[O]_{col}$ is explained by the solar and geomagnetic
521 activity. The linear trend for three midlatitude stations is negative but statistically
522 insignificant, whereas Sodankylä reveals a statistically significant negative trend of $n[O]_{col}$
523 but this trend might be artifact due to not considering particle precipitation.

524

525

526 **5 Ionosphere**

527

528 Research activity in the field of ionosphere has been more intense than in the
529 thermosphere. It has been focused on the F2 region, particularly on foF2 trends both due to
530 importance of foF2 and availability of the longest and relatively reliable data sets. Some
531 activity was also in the E-region ionosphere trend area. The first trend results were published
532 for electron density in the topside ionosphere. On the other hand, there was little progress in
533 the D-region trends since review by Laštovička and Bremer (2004) and no activity in the
534 previous five years.

535 Danilov and Konstantinova (2018) analyzed long-term trends in foE for stations Juliusruh
536 and Slough/Chilton; they found trends -0.12 and -0.05 MHz/decade, respectively for yearly
537 values and negative trends also for all months for the period after 1980.

538 Danilov and Konstantinova (2019) analyzed long-term changes of foE from stations
539 Juliusruh, Slough/Chilton, Rome, Moscow and Wakkanai. They found strong local-time



540 dependence of foE trend for Juliusruh shown in Fig. 4 with positive trends in the morning
541 sector, no trend at 11:00 LT and negative and stronger trends in the afternoon. The
542 dependence of foE trend on LT is much weaker for Rome (lower latitude). Seasonally the
543 trends reach maximum in December-January and minimum in July-August for Juliusruh (Fig.
544 4). The magnitude of foE trends clearly depends on geomagnetic latitude (Juliusruh and
545 Slough/Chilton 54°N, Moscow 51°N, Rome 42°N and Wakkanai 36°N); trend weakens with
546 decreasing latitude. This finding Danilov and Konstantinova (2019) consider evidence
547 supporting the impact of meridional transport of NO from auroral zone on observed trends in
548 foE.

549

550 **Figure 4.**

551

552 Givishvili and Leshchenko (2022) used data of Moscow and five Japanese stations to
553 search for long-term trend in the E region response to solar flares over 1969-2015. From their
554 analysis they derived the stable long-term increase of ratio of ionization rates $q_x/(q_x + q_{EUV})$ in
555 the E-region (q_x - soft X-ray ionization rate; q_{EUV} – solar EUV ionization rate) ; the ratio since
556 1969 approximately doubled in 2015. The increase was continuous, independent of solar
557 cycle, season or latitude. 74 years of observations at Moscow provide small but insignificant
558 increase of foE and relatively large and significant decrease of h'E (apparent height of the E-
559 layer maximum).

560 The first results on long-term trends in the topside ionosphere based on DMSP (Defense
561 Meteorological Satellite Program) satellite data over 1995-2017 were reported by Cai et al.
562 (2019). They found the electron density trend near 860 km around 18:00 MLT (Magnetic
563 Local Time) to have mean magnitude ranging from -2 to +2 %/decade with a clear seasonal,
564 latitudinal and longitudinal variation. The TIE GCM (Thermosphere-Ionosphere-
565 Electrodynamics General Circulation Model) simulated trends at 500 km have a similar
566 geographic distribution at 18 MLT. Simulations also suggest that the predominant electron
567 density trend driver at 500 km is the secular change of the Earth's magnetic field.

568 Zhou et al. (2022) investigated impact of increasing anthropogenic emissions on the
569 occurrence of equatorial plasma bubbles (EPBs) via simulating the growth rate of the
570 Rayleigh-Taylor instability, which is closely related to EPB generation. They used the Global
571 Coupled Ionosphere-Thermosphere-Electrodynamics Model of the Institute of Geology and
572 Geophysics, Chinese Academy of Sciences. With increasing CO₂ concentration the growth
573 rate significantly increases at low altitudes below about 260 km, decreases at high altitudes



574 above about 320 km, and between 260 km and 320 km increases (decreases) before (after)
575 midnight, indicating possible impact on radio communication systems. These changes are
576 caused by gravity and electrodynamic term, not by neutral wind.

577 Zhang et al. (2018) found that the results of Perrone and Mikhailov (2017 – PM17) on
578 exospheric temperature, which were based solely on foF1 measurements, were flawed and
579 quantitatively unlikely. They also showed that the conclusions of PM17 on long-term analysis
580 of ion temperatures derived from the incoherent scatter radar measurements are incorrect,
581 partly due to misunderstanding of nature of the incoherent scatter radar measuring process.

582 The remaining papers deal with long-term trends in the F2-region, mainly in foF2 but
583 partly also in hmF2.

584 An analysis of a 70-years long homogenized series (1947-2017) of observations of
585 ionosonde at Wuhan (30°N, central China) by Yue et al. (2018) found a weak but statistically
586 significant average negative trend in foF2, -0.021 MHz/decade, which varied with local time
587 from negative to slightly positive. The observed trends are attributed primarily to the secular
588 change of the Earth's magnetic field with CO₂ being the second important driver. As for
589 hmF2, the average trend is -1.06 km/decade with comparable role of CO₂ and Earth's
590 magnetic field (Yue et al., 2018).

591 Sharan and Kumar (2021) examined long-term foF2 variations from SH stations Hobart,
592 Canberra (35.3°S, 149.1°E) and Christchurch (43.5°S, 172.6°E) over 1947-2006. They found a
593 decrease of foF2 by 0.1-0.4 MHz per five solar cycles mainly due to increasing concentration
594 of CO₂; the midday trends were more significant and agreed better with model-inferred
595 expectations than midnight trends.

596 When the solar cycle 24 is included into nighttime foF2 long-term trends for stations
597 Wakkanai (45.4°N, 141.7°E) and Kokubunji (35.7°N, 139.5°E), the trends become less
598 negative, likely due to application of F10.7 as solar activity proxy (De Haro Barbas et al.,
599 2020). The trend weakening is less pronounced when Mg II is used as solar activity proxy
600 instead of F10.7.

601 Danilov and Konstantinova (2020c) found for Juliusruh that the pronounced negative
602 trends of hmF2 and foF2 persisted until 2002-2003, then they were followed by a vague
603 period with chaotic changes and in the most recent years a negative trend appeared again.

604 Sergeenko (2021) analyzed significant deviations (>20%) of foF2 (Δ foF2) from 10-day
605 median for stations Moscow (55.5°N, 37.3°E), Slough/Chilton (51.5°N, 01°W) and Hobart
606 (42.9°S, 147.3°E) for the period 1948-2010. They found that the maximum amplitudes of
607 positive Δ foF2 increased since the early 1980s at all stations in winter and except Moscow



608 also in summer, whereas for negative Δf_oF2 there was no change in Chilton and Hobart and
609 some increase in Moscow (particularly in summer). The increasing trend in positive Δf_oF2 is
610 likely related to changes in thermospheric wind system (Sergeenko, 2021).

611 The role of secular change of the Earth's magnetic field in long-term trends in F2 region
612 has also been studied but these results are reported in section 7. The results on selection of the
613 optimum solar activity proxies for F2 region trend studies are reported in section 2.

614 Significant progress was reached in long-term trends in the E-region ionosphere, namely in
615 foE. These trends were found to depend principally on local time up to their sign; this
616 dependence is strong at European high midlatitudes but much less pronounced at European
617 low midlatitudes, it is stronger in winter than in summer. Trends in foE also weaken with
618 decreasing geomagnetic latitude of station.

619 In the ionospheric F2-region very long data series (starting at 1947) of foF2 at NH as well
620 as SH revealed very weak but statistically significant negative trends. Some problems with
621 foF2 and hmF2 in were indicated in solar cycle 24, particularly towards its end.

622 First results on long-term trends in the topside ionosphere electron densities (trends
623 ranging from -2 to +2 %/decade at 840 km) and in the equatorial plasma bubbles (height-
624 dependent sign of trends) were reported.

625

626

627 **6 Global or Very-Long-Term Modeling**

628

629 Solomon et al. (2019) realized the first global simulation with model WACCM-X of
630 changes of temperature excited by anthropogenic trace gases simultaneously from surface to
631 the base of exosphere. They found that the anthropogenic cooling begins in the lower
632 stratosphere and it becomes dramatic, almost -2 K/decade, for the global mean zonal mean
633 temperature in the thermosphere. Only near the mesopause the cooling approaches zero
634 values. This pattern qualitatively agrees with observations. The temperature trend in the
635 thermosphere is somewhat stronger in the solar cycle minimum compared to the solar cycle
636 maximum conditions, likely due to the behavior of NO and O(³P) infrared irradiance
637 compared to that of CO₂.

638 Cnossen (2022) used model WACCM-X to simulate climate change in the upper
639 atmosphere (90-500 km) for the period 1950-2070 with moderate emission scenario SSP2-4.5
640 (Shared Socio-economic Pathway), secular change of the Earth magnetic field and reasonable
641 solar radiative and particle forcing in order to get the climate projection into the 21st century.



642 The obtained trends of thermospheric temperature (cooling) and density (reduction) are twice
643 as large in 2015-2070 as in historical period due to the more rapid absolute increase of CO₂
644 concentration. Trends in ionospheric parameters also become substantially stronger. However,
645 they display considerable spatial variability due to the secular change of the Earth's magnetic
646 field. The strongest ionospheric changes are expected in the region of 50°S-20°N and 90°-
647 0°W.

648 Yue et al. (2022) for the first time expanded simulations of the ionosphere over the whole
649 Holocene (9455 BCE – 2015 CE) with the Coupled Ionosphere-Thermosphere-
650 Electrodynamics model of the Chinese Institute of Geology and Geophysics driven by
651 realistic geomagnetic field, CO₂ levels and solar activity. They found that oscillations of the
652 global mean ionospheric profile are characterized by effects of geomagnetic field, decrease
653 (increase) of electron density above (below) ~200 km due to increasing CO₂ concentration,
654 and violent oscillations in phase with solar activity; the corresponding contributions to overall
655 variability being about 20%, 20% and 60%, respectively. The CO₂ effect is becoming non-
656 negligible and significant after ~1800 CE. The increase of CO₂ by 400 ppmv resulted in
657 simulated decrease of foF2 by 1.2 MHz, hmF2 by 34 km, and TEC by 4 TECU.

658 Garcia et al. (2019) simulated middle atmosphere temperature trends in the 20th and 21st
659 centuries with model WACCM. They investigated bi-decadal changes of temperature trend
660 profiles with the RCP 6.0 scenario of the greenhouse gas concentration evolution and found
661 the biggest change between 1975-1995 and 1995-2015, which is attributed to loss and
662 recovery of stratospheric ozone due to changing emissions of anthropogenic halogens. After
663 2015 the development of profile of temperature trends is controlled mainly by non-ODS
664 greenhouse gases.

665 Trends in temperature in the whole atmosphere from surface to the exosphere were
666 simultaneously simulated for the first time. The simulation confirmed the observed height-
667 dependent pattern of trends. Very long-period simulations of the middle atmosphere,
668 thermosphere and ionosphere confirmed acceleration of the trends during several last decades,
669 and it provided the first information about possible trends over the whole Holocene.

670

671

672 **7 Non-CO₂ Drivers of Trends**

673

674 The increasing concentration of CO₂ is not the only driver of long-term trends in the upper
675 atmosphere (e.g., Laštovička, 2017). At present the effect of secular change of Earth's



676 magnetic field and anthropogenic changes of stratospheric ozone are considered to be the
677 most important additional trend drivers in the ionosphere-thermosphere-mesosphere system.
678 Other driver's roles are also discussed, e.g. geomagnetic activity, atmospheric waves coming
679 from below, or water vapor (only in the mesosphere). Solar activity also changes on long-term
680 scales but because we need to remove solar cycle effect from (particularly ionospheric) data
681 before calculating trends, the solar activity effect is largely removed from trend calculations.
682 Let us start with the secular change of magnetic field, because its effects were relatively
683 broadly studied in the period 2018-2022.

684 Cnossen (2020) performed a long-term (1950-2015) simulation of the upper atmosphere
685 with model WACCM-X with realistic variation of solar and geomagnetic activity, changes of
686 the main magnetic field, and trace gas emissions including CO₂. The results confirm that CO₂
687 is the main driver of trends in thermospheric temperature and density, even though at high
688 magnetic latitudes the secular change of geomagnetic field plays also a role, particularly at
689 NH. Spatial patterns of trends in hmF₂, NmF₂ and TEC indicates the superposition of effects
690 of CO₂ and secular change of geomagnetic field, the latter being dominant in about 50°S-20°N
691 and 60°W-20°E. This longitudinal sector suffers with the largest change of the magnetic
692 equator position (e.g., Cnossen, 2020).

693 Qian et al. (2021) simulated long-term trends in the upper atmosphere using model
694 WACCM-X. They found that trends caused by both the secular change of geomagnetic field
695 but also the increasing concentration of CO₂ exhibit significant latitudinal and longitudinal
696 variability, which was not expected for CO₂. Thermospheric trends in density and temperature
697 are quite predominantly driven by greenhouse gases (GHGs); the secular change of
698 geomagnetic field plays some role in temperature trends in 120°W-20°E. In this longitudinal
699 sector, the secular change of geomagnetic field plays comparable role with GHGs in trends in
700 hmF₂, NmF₂ and Te and in Ti above 320 km while below 320 km the Ti trend is dominated
701 by GHGs. Figure 5 shows the changes of neutral density, neutral temperature T_n, electron
702 temperature Te and ion temperature Ti from the 1960s to the 2010s. The neutral temperature
703 and density change is clearly dominated by GHGs, whereas in Te and Ti in some regions the
704 effect of the secular change of magnetic field plays the dominant role. The secular change of
705 geomagnetic field is an important driver in sector 120°W-20°E but it excites locally both
706 positive and negative trends, consequently in global average trends its contribution is
707 negligible.

708

709 **Figure 5**



710

711 Simulations with the TIE GCM model (Cai et al., 2019) suggest that the predominant
712 electron density trend driver at 500 km is the secular change of the Earth's magnetic field.

713 During the next 50 years the dipole momentum of the Earth's magnetic field is predicted to
714 decrease by ~3.5%, the South Atlantic magnetic anomaly will expand, deepen and drift
715 westward, and magnetic dip poles will also move, which according to simulations with model
716 TIE-GCM will have impact on the thermosphere-ionosphere changes from 2015 to 2065
717 (Cnossen and Maute, 2020). The global mean thermospheric density should slightly increase
718 by ~1% in average and by up to 2% during magnetically disturbed conditions ($K_p \geq 4$),
719 particularly at SH. Global TEC should changes in the range -3% to +4% pending on season
720 and UT but regional changes may be up to $\pm 35\%$ in 45°S - 45°N , 110°W - 0°W during daytime,
721 mainly due to changes in the vertical $\mathbf{E} \times \mathbf{B}$ drift. The equatorial ionization anomaly will
722 weaken in sector ~ 105 - 60°W . The predicted changes of neutral density are very small
723 compared to effects of other trend drivers (mainly CO_2) but the predicted changes in TEC
724 might be regionally substantial.

725 As concerns observational results, Yue et al. (2018) found a weak but statistically
726 significant average negative trend in foF2 from 70 years of data at Wuhan (central China),
727 which they attributed primarily to the secular change of the Earth's magnetic field with CO_2
728 being the second important driver.

729 Other discussed topic is the impact of geomagnetic activity on CO_2 -driven trends in the
730 thermosphere and ionosphere. One paper dealt with long-term changes in NO radiative
731 cooling of the thermosphere.

732 Liu et al. (2021) used model GAIA to simulate the impact of geomagnetic activity on CO_2 -
733 driven trends in the thermosphere and ionosphere. They found that the thermospheric density
734 is the most robust indicator of the effect of CO_2 . The geomagnetic activity can either weaken
735 or strengthen CO_2 -driven trends in hmF2 and NmF2 depending on time and latitude. There is
736 interdependency between forcing by CO_2 and by geomagnetic activity; the efficiency of CO_2
737 forcing is higher under low than under high levels of geomagnetic activity forcing, and under
738 conditions of high CO_2 concentration the geomagnetic forcing is more efficient.

739 Chen et al. (2022) found that the geomagnetic activity-induced long-term change of foF2 is
740 seasonally discrepant. With long-term increase of geomagnetic activity foF2 increases in
741 winter while decrease in summer at middle and low latitudes; foF2 decreases at higher
742 latitudes whereas turns to increases with decreasing latitude in equinox. The linear trend
743 component is dominated by a long-term decreasing trend, which is in line with the increasing



744 greenhouse gas concentration. The geomagnetic activity in the most recent decades has a
745 decreasing trend, which has to be considered when the linear trend of foF2 is calculated to
746 estimate the impact of greenhouse gases.

747 Lin and Deng (2019) studied the role of NO in the climatology of global energy budget
748 and found that from 1982 to 2013 the decadal change of NO cooling reached ~25% of change
749 of total heating in the thermosphere below 150 km (its importance decreases with increasing
750 height) based on simulations with the Global Ionosphere-Thermosphere Model (GITM;
751 simulations were run for constant CO₂). However, the decadal change of NO cooling was
752 mainly due to decreasing solar (F10.7) and geomagnetic (Ap) activities.

753

754

755 **8 Conclusions**

756

757 This article reviews progress in long-term trends in the mesosphere-thermosphere-
758 ionosphere system reached over the period 2018-2022. Overall this progress may be
759 considered significant. The most active research was reached in the area of trends in the
760 mesosphere and lower thermosphere (MLT). Also research areas of problems in trend
761 calculations, global modeling and non-CO₂ drivers of long-term trends have been reviewed.
762 The main results are as follows:

763 Trends in the MLT region were relatively broadly studied. The contradictions about long-
764 term trends of concentration of CO₂ derived from satellite measurements was finally solved,
765 which is the result of principal importance. It was found that the CO₂ concentration trends in
766 the MLT region below 90 km do not differ statistically from trends at surface, even though
767 they appear to be slightly larger at heights above 90 km. The most studied parameter was
768 temperature. Huang and Mayr (2021) found that trends might significantly vary with local
769 time and height in the whole height range of 30-110 km but they studied data series only 13
770 years long. However, She et al. (2019) claim that data sets longer than two solar cycles are
771 necessary to obtain reliable long-term temperature trend. Model simulations confirm general
772 cooling, even though the WACCM simulations by Qian et al. (2019) indicate that the
773 temperature trend becomes near none or even slightly positive in the summer upper
774 mesosphere, likely due to dynamic effects. The results on temperature trends are generally
775 consistent with older results but develop and detailed them further.

776 Other important group in the MLT region is dynamical parameters, winds and atmospheric
777 waves. Here the trend pattern is much more complex. Observational data indicate different



778 wind trends up to sign of trend in different geographic regions, which is supported by model
779 simulations. The limited activity in the area of atmospheric waves was concentrated on tides.
780 Meteor radar wind data from high/middle latitudes revealed no significant trend in diurnal
781 tides and changes of semidiurnal tide, which differ according to altitude and latitude. On the
782 other hand, simulations with WACCM6 provide positive trends for both migrating and non-
783 migrating diurnal tides. Water vapor concentration trends in the mesosphere are generally
784 positive, only in the equatorial region there is almost no trend. As for long-term trends in the
785 related noctilucent clouds (NLCs), water vapor concentration was found to be the main driver
786 of trends in brightness and occurrence frequency, whereas cooling through mesospheric
787 shrinking is responsible for slight decrease in NLC heights. The polar mesospheric summer
788 echo trend was found to be positive, which might be related to the observed negative trend of
789 mesospheric temperatures in polar latitudes.

790 The research activity in the thermosphere was substantially lower. The negative trend of
791 thermospheric density continues without any evidence of clear dependence on solar activity.
792 The decrease in thermospheric density will result in increasing concentration of dangerous
793 space debris on LEO (Low Earth Orbit) satellite orbits. GAIA model simulations of trends in
794 many thermospheric parameters predict among others a downward shift and acceleration of
795 meridional circulation and substantial reduction of semidiurnal tides; both have not yet been
796 studied observationally.

797 Significant progress was reached in long-term trends in the E-region ionosphere, namely in
798 foE. These trends were found to depend principally on local time up to their sign; this
799 dependence is strong at European high midlatitudes but much less pronounced at European
800 low midlatitudes. In the ionospheric F2-region very long data series (starting at 1947) of foF2
801 at NH as well as SH revealed very weak but statistically significant negative trends. Some
802 problems with foF2 and hmF2 were indicated in solar cycle 24, particularly towards its end.
803 First results on long-term trends were reported for two new parameters, the topside
804 ionosphere electron densities (near 840 km) and the equatorial plasma bubbles.

805 Important part of long-term trend investigation is specification of roles of individual trend
806 drivers. The most important driver is the increasing concentration of CO₂ but other drivers
807 also play a role. The most studied one in the last five years was the effect of the secular
808 change of the Earth's magnetic field. The results of extensive modeling are mutually
809 qualitatively consistent. They reveal the dominance of secular magnetic change in trends in
810 foF2, hmF2, TEC and Te in the sector of about 50°S-20°N and 60°W-20°E. However, its
811 effect is locally both positive and negative, so in the global average this effect is negligible. In



812 the neutral atmosphere parameters the effects of the secular change of Earth's magnetic field
813 are much smaller. Model simulations of the geomagnetic activity impact show that it can
814 either weaken or strengthen CO₂-driven trends in hmF2 and NmF2 depending on time and
815 latitude and that its effect is seasonally discrepant.

816 Modeling provided some results not included in topical sections. Solomon et al. (2019)
817 realized the first global simulation with model WACCM-X of changes of temperature excited
818 by anthropogenic trace gases simultaneously from surface to the base of exosphere. The
819 results are generally consistent with observational pattern of trends. Very long-term modeling
820 yields trends of thermospheric temperature and density, which are twice as large in the 21st
821 century as trends in historical period due to more rapid absolute increase of CO₂
822 concentration. Simulation of ionospheric trends over the whole Holocene was reported for the
823 first time.

824 There are various problems in calculating long-term trends. They can be divided into three
825 groups: (1) natural variability, (2) data problems, and (3) methodology. These problems were
826 reviewed by Laštovička and Jelínek (2019). Main progress in the last five years was reached
827 by shedding light on problems related to natural variability, mainly on the problem of
828 removing/suppression of effect of solar cycle using various solar activity proxies, and also in
829 specifying problems of solar cycle 24 (2009-2019).

830 New findings contribute to improvement and broadening of scenario of long-term trends
831 in the upper atmosphere and ionosphere. Time is approaching when it will be possible to
832 construct a joint trend scenario of trends in the stratosphere-mesosphere-thermosphere-
833 ionosphere system.

834 Despite of evident progress, various challenges and open problems remain. The key
835 problem is the long-term trends in dynamics, particularly in activity of atmospheric waves,
836 which are very important component of vertical coupling in the atmosphere and which affect
837 all layers of the upper atmosphere. At present we only know that these trends might be
838 regionally different, even opposite. The atmospheric wave activity trend pattern seems to be
839 complex and the amount of observational data and also of studies dealing with wave trends is
840 insufficient. There are also challenges in further improvement of models for long-term trend
841 investigations and their interpretation. There is for example a difference in thermospheric
842 neutral density trends under low solar activity conditions between observations and
843 simulations; these trends affect lifetimes of dangerous space debris. Long-term trend in TEC
844 with implications to GNSS signal propagation and its applications in positioning and other
845 areas is not well known and understood and related trends in ionospheric scintillations are not



846 known at all. The role of majority potential non-CO₂ drivers of long-term trends in the upper
847 atmosphere is known only very qualitatively and needs to be more specified. Various water
848 vapor observational and model trends are not mutually sufficiently consistent. Trends in
849 various parameters depend on local time and season, which has not been sufficiently studied.
850 Summing up, a lot of work was done but a lot of work is still ahead.

851

852

853 **Data availability.** No data sets were used in this article.

854

855 **Competing interest.** The author has no competing interests.

856

857 **Financial support.** This research has been supported by the Czech Science Foundation under
858 grant 21-03295S.

859

860

861 **References**

862

863 Aikin, A. C., Chanin, M. L., Nash, J., and Kendig, D. J.: Temperature trends in the lower
864 mesosphere. *Geophys. Res. Lett.*, 18, 416-419, 1991.

865 Ardalan, M., Keckhut, P., Hauchecorne, A., Wing, R., Meftah, M., and Farhani, G.: Updated
866 climatology of mesospheric temperature inversions detected by Rayleigh lidar above
867 Observatoire de Haute Provence, France, using a K-mean clustering technique,
868 *Atmosphere*, 13(5), #814, <https://doi.org/10.3390/atmos13050814>, 2022.

869 Bailey, S. M., Thurairajah, B., Hervig, M. E., Siskind, D. E., Russell, J. M. III, and Gordley,
870 L. L.: Trends in the polar summer mesosphere temperature and pressure altitude from
871 satellite observations, *J. Atmos. Sol.-Terr. Phys.*, 220, 105650,
872 <https://doi.org/10.1016/j.jastp.2021.105650>, 2021.

873 Bizuneh, C. L., Prakash Raju, U. J., Nigussie, M., and Guimaraes Santos, C. A.: Long-term
874 temperature and ozone response to natural drivers in the mesospheric regions using 16
875 years (2005-2022) of TIMED/SABER observation data at 5-15°N, *Adv. Space Res.*, 70,
876 2095-2111, <https://doi.org/10.1016/j.asr.2022.06.051>, 2022.

877 Brown, M. K., Lewis, H. G., Kavanagh, A. J., and Cnossen, I.: Future decreases in
878 thermospheric neutral density in low Earth orbit due to carbon dioxide emissions, *J.*



- 879 Geophys. Res. Atmos., 126(8), e2021JD034589, <https://doi.org/10.1029/2021JD034589>,
880 2021.
- 881 Cai, Y., Yue, X., Wang, W., Zhang, S.-R., Liu, L., Liu, H., and Wan, W.: Long-term trend of
882 topside electron density derived from DMSP data during 1995-2017, *J. Geophys. Res.*
883 *Space Phys.*, 124, 10708-10727, <https://doi.org/10.1029/2019JA027522>, 2019.
- 884 Chen, Y., Liu, L., Le, H., Zhang, H., and Zhang, R.: Seasonally discrepant long-term
885 variations of the F2-layer due to geomagnetic activity and modulation to linear trend, *J.*
886 *Geophys. Res. Space Phys.*, 127(11), e2022JA030951,
887 <https://doi.org/10.1029/2022JA030951>, 2022.
- 888 Cicerone, R. J.: Greenhouse cooling up high. *Nature*, 344, 104-105, 1990.
- 889 Cnossen, I.: Analysis and attribution of climate change in the upper atmosphere from 1950 to
890 2015 simulated by WACCM-X. *J. Geophys. Res. Space Phys.*, 125(12), e2020JA028623,
891 <https://doi.org/10.1029/2020JA028623>, 2020.
- 892 Cnossen, I.: A realistic projection of climate change in the upper atmosphere into the 21st
893 century, *Geophys. Res. Lett.*, 49(19), e2022GL100693,
894 <https://doi.org/10.1029/2022GL100693>, 2022.
- 895 Cnossen, I., and Maute A.: Simulated trends in the ionosphere-thermosphere climate due to
896 predicted main magnetic field changes from 2015 to 2065. *J. Geophys. Res. Space Phys.*,
897 125(3), e2019JA027738, <https://doi.org/10.1029/2019JA027738>, 2020.
- 898 Dalla Santa, K., Orbe, C., Rind, D., Nazarenko, L., and Jonas, J.: Dynamical and trace gas
899 responses of the quasi-biennial oscillation to increased CO₂, *J. Geophys. Res. Atmos.*,
900 126(8), e2020JD034151, <https://doi.org/10.1029/2020JD034151>, 2021.
- 901 Dalin, P., Perminov, V., Pertsev, N., and Romejko, V.: Updated long-term trends in
902 mesopause temperature, airglow emissions, and noctilucent clouds, *J. Geophys. Res.*
903 *Atmos.*, 125(5), e2019JD030814, <https://doi.org/10.1029/2019JD030814>, 2020.
- 904 Danilov, A. D. Behavior of F2 region parameters and solar activity indices in the 24th cycle,
905 *Adv. Space Res.*, 67, 102-110, <https://doi.org/10.1016/j.asr.2020.09.042>, 2021.
- 906 Danilov, A. D., and Berberova, N. A.: Some applied aspects of the study of trends in the
907 upper and middle atmosphere, *Geomagn. Aeron.*, 61, 578-588,
908 <https://doi.org/10.1134/S0016793221040046>, 2021.
- 909 Danilov, A. D., and Konstantinova, A. V.: Long-term trends in the critical frequency of the E-
910 layer, *Geomagn. Aeron.*, 58, 338-347, doi: 10.1134/S0016793218030052, 2018.



- 911 Danilov, A. D., and Konstantinova, A. V.: Diurnal and seasonal variations in long-term
912 changes in the E-layer critical frequency, *Adv. Space Res.*, 359-370,
913 <https://doi.org/10.1016/j.asr.2018.10.015>, 2019.
- 914 Danilov, A. D., and Konstantinova, A. V.: Long-term variations of the parameters of the
915 middle and upper atmosphere and ionosphere (review), *Geomagn. Aeron.*, 60, 397-420,
916 <https://doi.org/10.1134/S0016793220040040>, 2020a.
- 917 Danilov, A. D., and Konstantinova, A. V.: Trends in parameters of the F2 layer and the 24th
918 solar activity cycle, *Geomagn. Aeron.*, 60, 586-596,
919 <https://doi.org/10.1134/s0016793220050047>, 2020b.
- 920 Danilov, A. D., and Konstantinova, A. V.: Trends in hmF2 and the 24th solar activity cycle,
921 *Adv. Space Res.*, 66, 292-298, <https://doi.org/10.1016/j.asr.2020.04.011>, 2020c.
- 922 Das, U.: Spatial variability in long-term temperature trends in the middle atmosphere from
923 SABER/TIMED observations, *Adv. Space Res.*, 68, 2890-2903,
924 <https://doi.org/10.1016/j.asr.2021.05.014>, 2021.
- 925 De Haro Barbas, B. F., Elias, A. G., Fagre, M., and Zossi, B. S.: Incidence of solar cycle 24 in
926 nighttime foF2 long-term trends for two Japanese ionospheric stations, *Studia Geoph.*
927 *Geod.*, 64, 407-418, <https://doi.org/10.1007/s11200-021-0584-9>, 2020.
- 928 Elias, A. G., De Haro Barbas, B. F., Zossi, B. S., Medina, F. D., Fagre, M., and Venchiaerutti,
929 J. V.: Review of long-term trends in the equatorial ionosphere due to geomagnetic field
930 secular variations and its relevance to space weather, *Atmosphere*, 13, #40,
931 <https://doi.org/10.3390/atmos13010040>, 2022.
- 932 Emmert, J. T., Picone, J. M., and Meier, R. R.: Thermospheric global average density trends
933 1967-2007, derived from orbits of 5000 near-Earth objects. *Geophys. Res. Lett.*, 35,
934 L05101 (2008), doi: 10.1029/2007GL032809.
- 935 French, W. J. R., Mulligan, F. J., and Klekociuk, A. R.: Analysis of 24 years of mesopause
936 region OH rotational temperature observations at Davis, Antarctica – Part 1: long-term
937 trends, *Atmos. Chem. Phys.*, 20, 6379-6394, <https://doi.org/10.5194/acp-20-6379-2020>,
938 2020.
- 939 Garcia, R. R., Yue, J., and Russell, J. M. III.: Middle atmosphere temperature trends in the
940 twenties and twenty-first centuries simulated with the Whole Atmosphere Community
941 Climate Model (WACCM), *J. Geophys. Res. Space Phys.*, 124, 7984-7993,
942 <https://doi.org/10.1029/2019JA026909>, 2019.



- 943 Givishvili, G. V., and Leshchenko, L. N.: Long-term trend of the ionospheric E-layer
944 response to solar flares, *Sol.-Terr. Phys.*, 8, 51-57, [https://doi.org/10.12737/stp-](https://doi.org/10.12737/stp-81202206)
945 [81202206](https://doi.org/10.12737/stp-81202206), 2022.
- 946 Huang, F. T., and Mayr, H. G.: Temperature decadal trends, and their relations to diurnal
947 variations in the lower thermosphere, stratosphere and mesosphere, based on
948 measurements from SABER on TIMED. *Ann. Geophys.*, 39, 327-339,
949 <https://doi.org/10.5194/angeo-39-327-2021>, 2021.
- 950 Huang, J., Hao, Y., Zhang, D., and Xiao, Z.: The use of monthly mean average for
951 investigating the presence of hysteresis and long-term trends in ionospheric NmF2. *J.*
952 *Geophys. Res. Space Phys.*, 125(1), e2019JA026905,
953 <https://doi.org/10.1029/2019JA026905>, 2020.
- 954 Huang, T.-Y.: Influences of CO₂ increase, solar cycle variation, and geomagnetic activity on
955 airglow from 1960-2015, *J. Atmos. Sol.-Terr Phys.*, 171, 164-175,
956 <https://doi.org/10.1016/j.jastp.2017.06.008>, 2018.
- 957 Jaen, J., Renkowitz, T., Chau, J. L., He, M., Hoffmann, P., Yamazaki, Y., Jacobi, C., Tsutsumi,
958 M., Matthias, V., and Hall, C.: Long-term studies of mesosphere and lower thermosphere
959 summer length definitions based on mean zonal wind features observed for more than one
960 solar cycle at middle and high latitudes in the Northern Hemisphere, *Ann. Geophys.*, 40,
961 23-35, <https://doi.org/10.5194/angeo-40-23-2022>, 2022.
- 962 Kuilman, M. S., Zhang, Q., Cai, M., and Weng, Q.: Using the climate feedback response
963 analysis method to quantify climate feedbacks in the middle atmosphere, *Atmos. Chem.*
964 *Phys.*, 20, 12409-12430, <https://doi.org/10.5194/acp-20-12409-2020>, 2020.
- 965 Kogure, M., Liu, H., and Tao, C.: Mechanisms for zonal mean wind responses in the
966 thermosphere to doubled CO₂ concentration, *J. Geophys. Res. Space Phys.*, 127(9),
967 e2022JA030643, <https://doi.org/10.1029/2022JA030643>, 2022.
- 968 Lainer, M., Hocke, K., Eckert, E., and Kämpfer, N.: Significant decline of mesospheric water
969 vapor at the NDACC site near Bern in the period 2007 to 2018, *Atmos. Chem. Phys.*, 19,
970 6611-6620, <https://doi.org/10.5194/acp-19-6611-2019>, 2019.
- 971 Latteck, R., Renkowitz, T., and Chau, J. L.: Two decades of long-term observations of polar
972 mesospheric echoes at 69°N, *J. Atmos. Sol.-Terr. Phys.*, 216, 105576,
973 <https://doi.org/10.1016/j.jastp.2021.105576>, 2021.
- 974 Laštovička, J.: A review of recent progress in trends in the upper atmosphere. *J. Atmos. Solar-*
975 *Terr. Phys.*, 163, 2–13, <https://doi.org/10.1016/j.jastp.2017.03.009>, 2017.



- 976 Laštovička, J.: Is the relation between ionospheric parameters and solar proxies stable?
977 *Geophys. Res. Lett.*, 46, 14208-14213, <https://doi.org/10.1029/2019GL085033>, 2019.
- 978 Laštovička, J.: What is the optimum solar proxy for long-term ionospheric investigations?
979 *Adv. Space Res.*, 67, 2-8, <https://doi.org/10.1016/j.asr.2020.07.025>, 2021a.
- 980 Laštovička, J.: The best solar activity proxy for long-term ionospheric investigations. *Adv.*
981 *Space Res.*, 68, 2354-2360. <https://doi.org/10.1016/j.asr.2021.06.032>, 2021b.
- 982 Laštovička, J.: Long-term changes of ionospheric climate in terms of foF2. *Atmosphere*,
983 13:110, <https://doi.org/10.3390/atmos13010110>, 2022.
- 984 Laštovička, J., Akmaev, R. A., Beig, G., Bremer, J., and Emmert, J. T.: Global change in the
985 upper atmosphere. *Science*, 314, 1253-1254, 2006.
- 986 Laštovička, J., Akmaev, R. A., Beig, G., Bremer, J., Emmert, J. T., Jacobi, C., Jarvis, M. J.,
987 Nedoluha, G., Portnyagin, Yu. I., and Ulich, T.: Emerging pattern of global change in the
988 upper atmosphere and ionosphere. *Ann. Geophysicae*, 26, 1255-1268,
989 <https://doi.org/10.5194/angeo-26-1255-2008>, 2008.
- 990 Laštovička, J., Bremer, J.: An overview of long-term trends in the lower ionosphere below
991 120 km. *Surv. Geophys.*, 25, 69–99,
992 <https://doi.org/10.1023/B:GEOP.0000015388.75164.e2>, 2004.
- 993 Laštovička, J., Jelínek, Š.: Problems in calculating long-term trends in the upper atmosphere.
994 *J. Atmos. Solar-Terr. Phys.*, 189, 80-86, <https://doi.org/10.1016/j.jastp.2019.04.011>,
995 2019.
- 996 Laštovička, J., and Pancheva, D.: Changes in characteristics of planetary waves at 80-100 km
997 over Central and Southern Europe since 1980. *Adv. Space Res.*, 11 (3), 31-34, 1991.
- 998 Li, T., Yue, J., Russell J. M. III, and Zhang, X.: Long-term trend and solar cycle in the middle
999 atmosphere temperature revealed from merged HALOE and SABER datasets. *J. Atmos.*
1000 *Sol.-Terr. Phys.*, 212, 105506, <https://doi.org/10.1016/j.jastp.2020.105506>, 2021.
- 1001 Lin, C.-Y., and Deng, Y.: Nitric oxide in climatological energy budget during 1982-2013. *J.*
1002 *Geophys. Res. Space Phys.*, 124, 782-789, <https://doi.org/10.1029/2018JA025902>, 2019.
- 1003 Liu, H., Tao, C., Jin, H., and Nakamoto, Y.: Circulation and tides in a cooler upper
1004 atmosphere: Dynamical effects of CO₂ doubling, *Geophys. Res. Lett.*, 47(10),
1005 e2020GL087413, <https://doi.org/10.1029/2020GL087413>, 2020.
- 1006 Liu, H., Tao, C., Jin, H., and Abe, T.: Geomagnetic activity effect on CO₂-driven trend in the
1007 thermosphere and ionosphere: Ideal model experiments with GAIA. *J. Geophys. Res.*
1008 *Space Phys.*, 126(1), e2020JA028607, <https://doi.org/10.1029/2020JA028607>, 2021.



- 1009 Lübken, F.-J., Berger, U., and Baumgarten, G.: On the anthropogenic impact on long-term
1010 evolution of noctilucent clouds, *Geophys. Res. Lett.*, 45, 6681-6689,
1011 <https://doi.org/10.1029/2918GL077719>, 2018.
- 1012 Lübken, F.-J., Baumgarten, G., and Berger, U.: Long-term trends of mesospheric ice layers”
1013 A model study, *J. Atmos. Sol.-Terr. Phys.*, 214, 105378,
1014 <https://doi.org/10.1016/j.jastp.2020.105378>, 2021.
- 1015 Mlynczak, M. G., Hunt, L. A., Garcia, R. R., Harvey, V. L., Marshall, B. T., Yue, J., Mertens,
1016 C. J., and Russell, J. M. III: Cooling and contraction of the mesosphere and lower
1017 thermosphere from 2002 to 2021, *J. Geophys. Res. Atmos.*, 127(22), e2022JD036767,
1018 <https://doi.org/10.1029/2022JD036767>, 2022.
- 1019 Nedoluha, G. E., Gomez, R. M., Boyd, I., Neal, H., Allen, D. R., Siskind, D. E., Lambert, A.,
1020 and Livesey, N. J.: Measurements of mesospheric water vapor from 1992 to 2021 at three
1021 stations from the Network for the Detection of Atmospheric Composition Change, *J.*
1022 *Geophys. Res. Atmos.*, 127(21), e2022JD037227, <https://doi.org/10.1029/2022JD037227>,
1023 2022.
- 1024 Perminov, V. I., Semenov, A. I., Pertsev, N. N., Medvedeva, I. V., Dalin, P. A., and
1025 Sukhodoev, V. A.: Multi-year behavior of the midnight OH* temperature according to
1026 observations at Zvenigorod over 2000-2016, *Adv. Space Res.*, 61, 1901-1908,
1027 <https://doi.org/10.1016/j.asr.2017.07020>, 2018.
- 1028 Perminov, V. I., Pertsev, N. N., Dalin, P. A., Zheleznov, Yu. A., Sukhodolev, V. A., and
1029 Orekhov, M. D.: Seasonal and long-term changes in the intensity of O₂(b¹Σ) and
1030 OH(X²Π) airglow in the mesopause region, *Geomagn. Aeron.*, 61, 589-599,
1031 <https://doi.org/10.1134/S0016793221040113>, 2021.
- 1032 Perrone, L., and Mikhailov, A. V.: Long-term variations of exospheric temperature inferred
1033 from foF1 observations: A comparison to ISR Ti trend estimates. *J. Geophys. Res. Space*
1034 *Phys.*, 122, 8883-8892, <https://doi.org/10.1029/2017JA024193>, 2017.
- 1035 Perrone, L., and Mikhailov, A. V.: Long-term variations of June column atomic oxygen
1036 abundance in the upper atmosphere inferred from ionospheric observations, *J. Geophys.*
1037 *Res. Space Phys.*, 124, 6305-6312, <https://doi.org/10.1029/2019JA026818>, 2019.
- 1038 Qian, L., Jacobi, C., and McInerney, J.: Trends and solar irradiance effects in the mesosphere,
1039 *J. Geophys. Res. Space Phys.*, 124, 1343-1360, <https://doi.org/10.1029/2018JA026367>,
1040 2019.
- 1041 Qian, L., McInerney, J. M., Solomon, S. S., Liu, H., and Burns, A. G.: Climate changes in the
1042 upper atmosphere: Contributions by the changing greenhouse gas concentrations and



- 1043 Earth's magnetic field from the 1960s to 2010s, *J. Geophys. Res. Space Phys.*, 126(3),
1044 e2020JA029067, <https://doi.org/10.1029/2020JA029067>, 2021.
- 1045 Ramesh, K., and Smith, A. K.: Long-term variability and tendencies in non-migrating diurnal
1046 tide from WACCM6 simulations during 1850-2014, *J. Geophys. Res. Space Phys.*,
1047 126(3), e2020JA028904, <https://doi.org/10.1029/2020JA028904>, 2021.
- 1048 Ramesh, K., Smith A. K., Garcia, R. R., Marsh, D. R., Sridharan, S., and Kishore Kumar, K.:
1049 Long-term variability and tendencies in migrating diurnal tide from WACCM6
1050 simulations during 1850-2014, *J. Geophys. Res. Atmos.*, 125(23), e2020JD033644,
1051 <https://doi.org/10.1029/2020JD033644>, 2020a.
- 1052 Ramesh, K., Smith A. K., Garcia, R. R., Marsh, D. R., Sridharan, S., and Kishore Kumar, K.:
1053 Long-term variability and tendencies in the middle atmosphere temperature and zonal
1054 wind from WACCM6 simulations during 1850-2014, *J. Geophys. Res. Atmos.*, 125(24),
1055 e2020JD033579, <https://doi.org/10.1029/2020JD033579>, 2020b.
- 1056 Rezac, L., Yue, J., Yongxiao, J., Russell, J. M., III, Garcia, R., López-Puertas, M., and
1057 Mlynczak, M. G.: On long-term SABER CO₂ trends and effects due to non-uniform
1058 space and time sampling, *J. Geophys. Res. Space Phys.*, 123, 7958–1967,
1059 <https://doi.org/10.1029/2018JA025892>, 2018.
- 1060 Rishbeth, H.: A greenhouse effect in the ionosphere? *Planet. Space Sci.*, 38, 945–948, 1990.
- 1061 Rishbeth, H., and Roble, R. G.: Cooling of the upper atmosphere by enhanced greenhouse
1062 gases - modelling of thermospheric and ionospheric effects. *Planet. Space Sci.*, 40, 1011-
1063 1026, 1992.
- 1064 Roble, R. G., and Dickinson, R. E.: How will changes in carbon dioxide and methane modify
1065 the mean structure of the mesosphere and lower thermosphere? *Geophys. Res. Lett.*, 16,
1066 1441–1444, 1989.
- 1067 Sergeenko, N. P.: Long-term dynamics of the properties of ionospheric F2-layer disturbances
1068 in various regions. *Geomagn. Aeron.*, 61, 234-240, <https://10.1134/S0016793221020158>,
1069 2021.
- 1070 Sharan, A., and Kumar, S.: Long-term trends of the F2 region at mid-latitudes in the Southern
1071 Hemisphere, *J. Atmos. So.-Terr. Phys.*, 220, 105683,
1072 <https://doi.org/10.1016/j.jastp.2021.105683>, 2021.
- 1073 She, C.-Y., Berger, U., Yan, Z.-A., Yuan, T., Lübken, F.-J., Krueger, D. A., and Hu, X.:
1074 Long-term trend of midlatitude mesopause region temperature based on 28 years (1990-
1075 2017) of Na lidar observations, *J. Geophys. Res. Space Phys.*, 124, 7140-7156,
1076 <https://doi.org/10.1029/2019JA026759>, 2019.



- 1077 Solomon, S. C., Liu, H.-L., Marsh, D. R., McInerney, J. M., Qian, L., and Vitt, F. M.: Whole
1078 atmosphere climate change: Dependence on solar activity, *J. Geophys. Res. Space Phys.*,
1079 124, 3799-3809, <https://doi.org/10.1029/2019JA026678>, 2019.
- 1080 Venkat Ratnam, M., Akhil Raj, S.T., and Qian, L.: Long-term trends in the low-latitude
1081 middle atmosphere temperature and winds: Observations and WACCM-X model
1082 simulations, *J. Geophys. Res. Space Phys.*, 124, 7320-7331,
1083 <https://doi.org/10.1029/2019JA026928>, 2019.
- 1084 Vincent, R. A., Kovalam, S., Murphy, D. J., Reid, I. M., and Younger, J. P.: Trends and
1085 variability in vertical winds in the Southern Hemisphere summer polar mesosphere and
1086 lower thermosphere, *J. Geophys. Res. Atmos.*, 124, 11070-11085,
1087 <https://doi.org/10.1029/2019JD030735>, 2019.
- 1088 Weng, L., Lei, J., Zhong, J., Dou, X., and Fang, H.: A machine-learning approach to derive
1089 long-term trends of thermospheric density, *Geophys. Res. Lett.*, 47(3), e2020GL087140,
1090 <https://doi.org/10.1029/2020GL087140>, 2020.
- 1091 Wilhelm, S., Stober, G., and Brown, P.: Climatologies and long-term changes in mesospheric
1092 wind and wave measurements based on radar observations at high and mid latitudes, *Ann.*
1093 *Geophys.*, 37, 851-875, <https://doi.org/10.5194/angeo-37-851-2019>, 2019.
- 1094 Yu, W., Garcia, R., Yue, J., Russell, J. III, and Mlynczak, M.: Variability of water vapor in
1095 the tropical middle atmosphere observed from satellites and interpreted using SD-
1096 WACCM simulations, *J. Geophys. Res. Atmos.*, 127(13), e2022JD036714,
1097 <https://doi.org/10.1029/2022JD036714>, 2022.
- 1098 Yuan, T., Solomon, S. C., She, C.-Y., Krueger, D. A., and Liu, H.-L.: The long-term trends of
1099 nocturnal mesopause temperature and altitude revealed by Na lidar observations between
1100 1990 and 2018 at midlatitude, *J. Geophys. Res. Atmos.*, 124, 5970-5980,
1101 <https://doi.org/10.1029/2018JD029828>, 2019.
- 1102 Yue, J., Russell, J. III, Gan, Q., Wang, T., Rong, P., Garcia, R., and Mlynczak, M.: Increasing
1103 water vapor in the stratosphere and mesosphere after 2002, *Geophys. Res. Lett.*, 46,
1104 13452-13460, <https://doi.org/10.1029/2019GL084973>, 2019.
- 1105 Yue, X., Hu, L., Wei, Y., Wan, W., and Ning, B.: Ionospheric trend over Wuhan during 1947-
1106 2017: Comparison between simulation and observation, *J. Geophys. Res. Space Phys.*,
1107 123, 1396-1409, <https://doi.org/10.1002/2017JA024675>, 2018.
- 1108 Yue, X., Cai, Y., Ren, Z., Zhou, X., Wei, Y., and Pan, Y.: Simulated long-term evolution of
1109 the ionosphere during Holocene, *J. Geophys. Res. Space Phys.*, 127(11),
1110 e2022JA031042, <https://doi.org/10.1029/2022JA031042>, 2022.



1111 Zhang, S.-R., Holt, J. M., Erickson, P. J., and Goncharenko, L. P.: Comments on “Long-term
1112 variations of exospheric temperatures inferred from foF1 observations: A comparison to
1113 ISR Ti trend estimates” by Perrone and Mikhailov, *J. Geophys. Res. Space Phys.*, 123,
1114 4467-4473, <https://doi.org/10.1029/2017JA024948>, 2018.

1115 Zhao, X. R., Sheng, Z., Shi, H. Q., Weng, L. B., and Liao, Q. X.: Long-term trends and solar
1116 responses of the mesopause temperatures observed by SABER during the 2002-2019
1117 period, *J. Geophys. Res. Atmos.*, 125(11), e2020JD032418,
1118 <https://doi.org/10.1029/2020JD032418>, 2020.

1119 Zhao, X. R., Sheng, Z., Shi, H. Q., Weng, L. B., and He, Y.: Middle atmosphere temperature
1120 changes derive from SABER observations during 2002-2020, *J. Clim.*, 34, 7995-8012,
1121 <https://doi.org/10.1175/JCLI-D-20-1010.1>, 2021.

1122 Zhou, X., Yue, X., Ren, Z., Liu, Y., Cai, Y., Ding, F., and Wei, Y.: Impact of anthropogenic
1123 emission changes on the occurrence of equatorial plasma bubbles, *Geophys. Res. Lett.*,
1124 49(3), e2021GL097354, <https://doi.org/10.1029/2021GL097354>, 2022.

1125

1126

1127

1128

1129 **Figure 1.** Yearly values of foF2 residuals after removing solar influence for Pruhonice, 1996-
1130 2014. Green curve - solar activity proxy F10.7; blue curve – solar proxy F30; red curve –
1131 solar proxy Mg II; longer-dash colored lines – respective linear trends; short-dash black
1132 horizontal line – zero difference level. A negative difference means smaller observed than
1133 model value. After Laštovička (2021b).

1134

1135 **Figure 2.** Temperature trends (K per decade) vs. altitude from 20 to 100 km at 20° N (a) and
1136 44° N (b). Black: trends based on SABER zonal means over longitude and local time; blue:
1137 based on zonal means at 00:00 LT; green: 06:00 LT, red: 12:00 LT, magenta: 18:00 LT. After
1138 Huang and Mayr (2021).

1139

1140 **Figure 3.** Average monthly mean zonal wind at 0.001 hPa (~90 km) for March, June,
1141 September, and December, simulated by model WACCM-X for the period of 2000–2014 (top
1142 row). The corresponding zonal wind trends (middle row). The corresponding solar irradiance
1143 effect on the zonal winds (lower row). After Qian et al. (2019).

1144



1145 **Figure 4.** Seasonal variations of the trend slope/coefficient of foE for various LT moments for
1146 Juliusruh station. Courtesy by Danilov and Konstantinova (2019).

1147

1148 **Figure 5.** Left panels show the global distributions of neutral temperature T_n at 300 km, ion
1149 temperature T_i at 300 km, electron temperature T_e at 400 km and neutral density ρ at 400 km
1150 in the 1960s. Right panels show changes of global distributions of these four parameters from
1151 the 1960s to the 2010s separately for the effect of greenhouse gases (GHGs, in the
1152 thermosphere essentially CO_2 , left part) and of the secular change of the Earth's magnetic
1153 field (right part). After Qian et al. (2021).

1154

1155

1156

1157

1158

1159

1160

1161

1162

1163

1164

1165

1166

1167

1168

1169

1170

1171

1172

1173

1174

1175

1176

1177

1178

1179

1180

1181

1182

1183

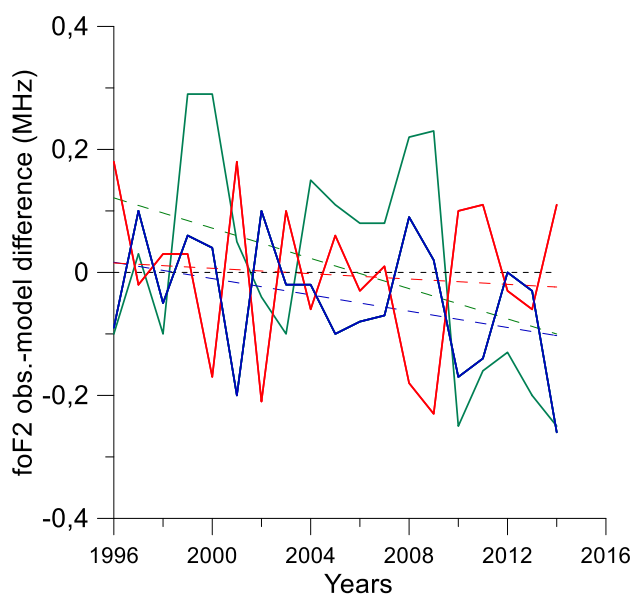
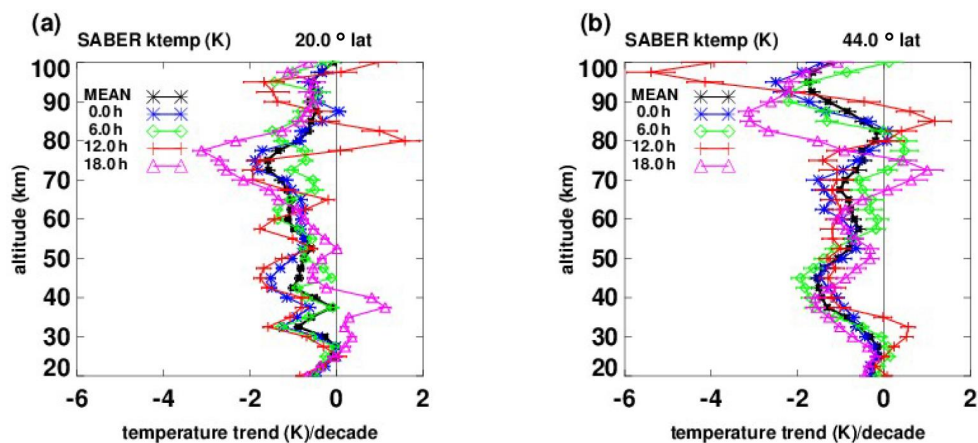


Fig. 1

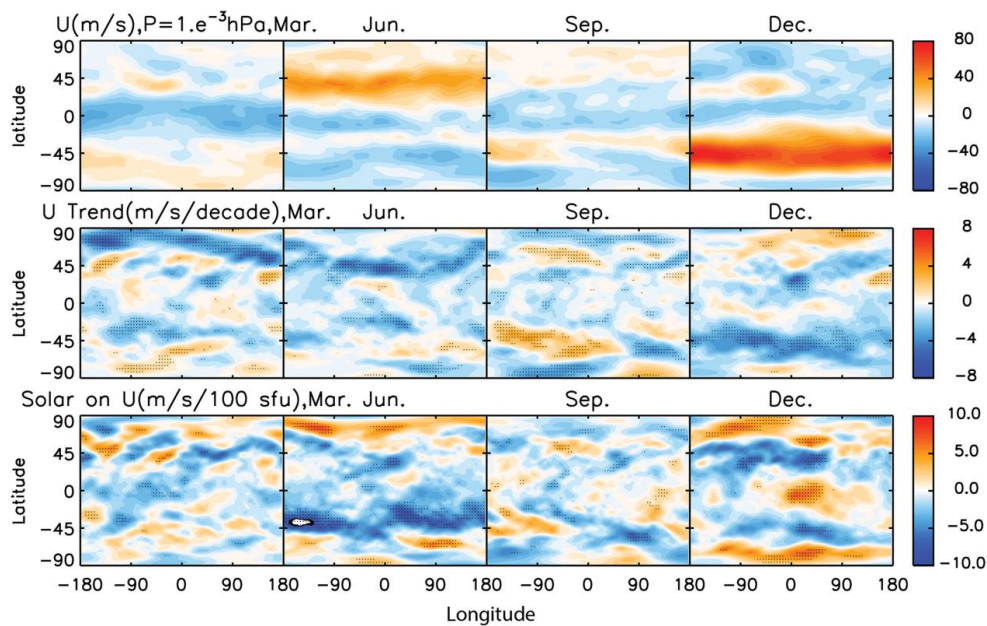


1184
1185



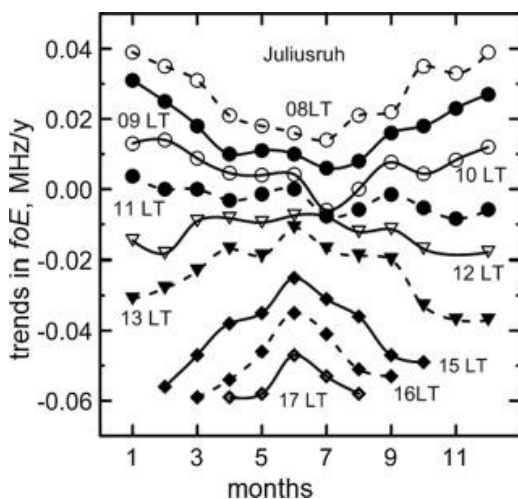
1186
1187
1188
1189
1190
1191

Fig. 2



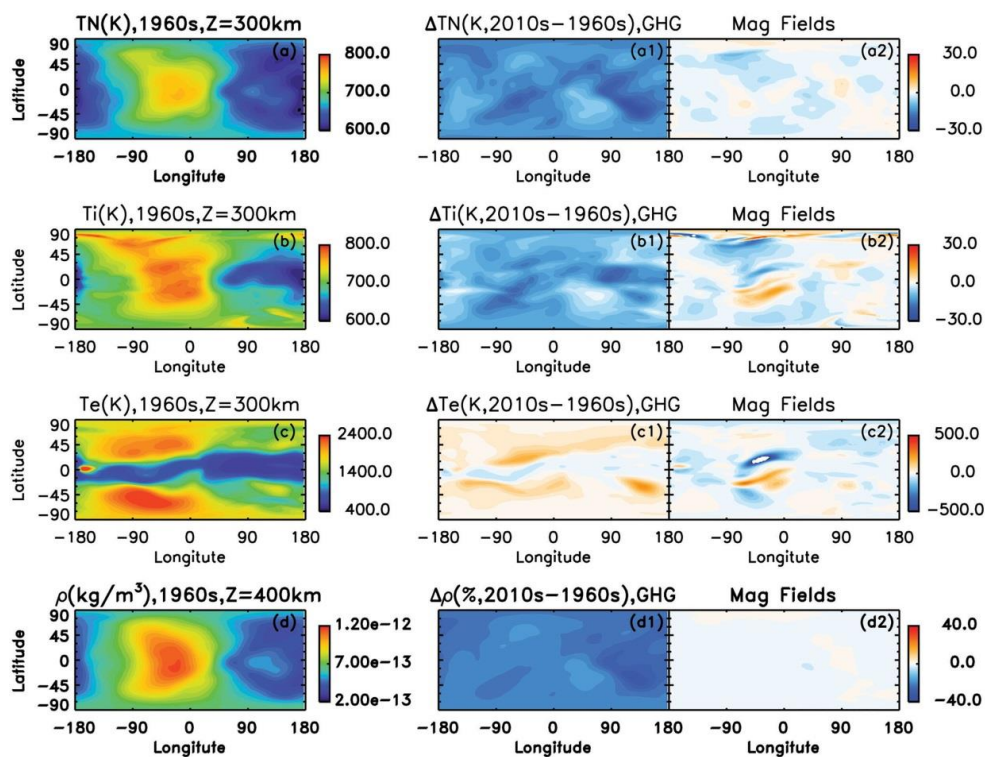
1192
1193
1194
1195
1196
1197
1198

Fig.3



1199
 1200
 1201
 1202
 1203

Fig. 4



1204
 1205
 1206
 1207

Fig. 5